ISSN 2303-4521
Periodicals of Engineering and Natural Sciences *Original Research*
Vol. 9, No. 3, July 2021, pp.335-344

Design of second order sliding mode observer based equivalent Back-EMF for rotor position estimation of PMSM

Maher Faeq[1], Nidam M. Abdul Majeed[2], Farah Z. Jasim[3]
[1,2,3] Electronic and Control Engineering, Kirkuk Technical College, Northern Technical University, Kirkuk. Iraq

ABSTRACT

This study introduces a scheme to estimate rotor position by the use of an Equal electromotive force (EMF) model of a synchronous machine. This use could be substituted by a sliding-mode observer (SMO) according to an equal EMF for superior reference speed tracking. There is an algorithm of the second order sliding-mode-control (SO-SMC) in controlling speed of permanent magnet synchronous motor (PMSM). This is by the use of the proportional plus-integral PI control sliding plane. The current work discusses the PMSM, which follows field-oriented appears. In addition, there are SO-SMC laws and PI sliding plans. This paper shows that the proposed high-speed PMSM sensorless speed control is valid by MATLAB simulations.

Keywords: sliding mode observer, rotor position estimation ,PMSM speed control

Corresponding Author:

Maher Faeq Mohammed
Kirkuk Technical College
Northern Technical University, Kirkuk, Iraq
E-mail: maher_usm@ntu.edu.iq

1. Introduction

Recently, PMSM drives have a very significant role in different speed uses such as in computer numerical control (CNC). It is also utilized in elevators and robots[1-4]. Field-oriented control (FOC) (sometimes called vector control) could help getting a rapid "four-quadrant operation" with a smooth starting and speed when designing PMSM servo drives. However, there are many electromechanical parameters, which are not yet exactly described. Also, it is changeable and could be disturbed in terms of external load while operating. This makes the drive performance degradates[5, 6]. For this drawback reduction, there are many suggested modern and intelligent control techniques for dealing with the uncertainties[7-11]. The control in the side mode is applied extensively and successfully to electrical drivers including PMSM servo drives because of the high degree of precision, simplicity and robustness. However, since the traditional FO-SMC chattering phenomenon was born from the interaction between parasite and high frequency switchover control, which is the most damaging implementation disadvantage of the SMC, it was little used in a high performance condition[12, 13]. A number of control schemes were proposed [14-16] to address this problem. This paper examines the characteristics of the SO-SMC Technique based on the PI sliding plane in order to combat the two phenomena and to preserve the main advantages of the SMC (precision, robustness). The contribution of this paper to the speed control of PMS M is successfully used by the SO-SMC. This paper is organized accordingly. First of all there is a FOC PMSM servo drive, and the mathematical model of the airplane is developed in a nominal condition. The theoretical analysis is then presented in detail for the sliding mode speed controller. Then a PMSM servo drive aircraft simulates the proposed slid-mode mode speed controller. In conclusion, the conclusions were drawn. The proposed sliding mode controller offers high-performance dynamic properties of trajectory precisely and robust in terms of variations of plant parameters and externals in load disturbances, depending on the simulation results from the testing of the PMSM servo drive speed controls.

2. PMSM servo system dynamic based field-oriented

PMSM, regarding its mathematics, in the reference frame of the rotor rotating can be [17].

$$v_q = R_s i_q + \dot{\lambda}_q + \omega_e \lambda_d \quad (1)$$

$$v_d = R_s i_d + \dot{\lambda}_d - \omega_e \lambda_q \quad (2)$$

$$\lambda_q = L_q i_q \quad (3)$$

$$\lambda_d i_d + L_{md} I_{df} \quad (4)$$

$$\omega_e = n_p \,.\, \omega_r \quad (5)$$

Where

v_d, v_q voltage of d.q-axis stator

i_d, i_q currents of d, q axis stator

λ_d, λ_q flux linkages of d, q axis stator.

L_d, L_q nnnd, q axis stator inductances.

ω_e inverter frequency.

ω_r rotor speed

L_{md} d- inductance of axis mutual

I_{df} magnetizing current of equivalent d-axis

n_p pole pair number.

R_s resistance of the stator

The motor dynamics and electric torques is as follows:

$$T_e = \frac{3}{2}\frac{p}{2}\left(\lambda_d i_q - \lambda_q i_d\right) \quad (6)$$

$$T_e = J\dot{\omega}_r + B_m \omega_r + T_L \quad (7)$$

Here, T_L stands for the load torque while T_e is the generated electromagnetic torque. In addition, there are $coefficient\ of\ viscosity\ B_m$ and J rotational inertia which is known as the moment of inertia. Fig.1 explains the field-oriented mechanism use for making "the speed loop control of the PMSM" servo drive system simple to regulate the block of the system where id stands for the forced to zero, (6):

$$T_e = K_p i^*_q \quad (8)$$

Here, i_q^* is the SO-SMC control output (iq). The field-oriented control PMSM servo drive configuration as Fig. 1 explains. It has a number of elements. The first is PM synchronous servo motor set. The second is Space Vector PWM voltage source inverter (VSI). The third could be the current controller. In addition, a triple coordinate translator, and a speed control loop (SO-SMC) are included explained next:

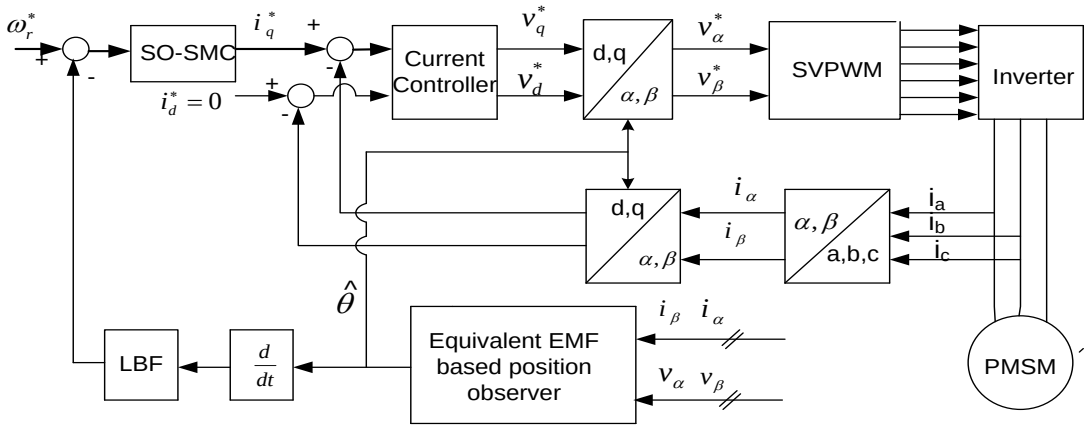

Figure 1. Control block with equivalent EMF

3. SO-SMC

The primary function of SO-SMC is the reduction the sliding plane with its first-order derivative to zero corresponding to the acting of the control which is the initial sliding plane derivative. Therefore, the literature includes various SO-SMC algorithms including the "twisting" and "super-twisting"[18-20], "two stage SMO" and "global" [21], discrete time observer algorithms [22-25]. Yet, these algorithms are only used theoretically. There is a lack of its use in PMSM control. Thus, this works uses SO-SMC within the field of the regulation of the speed of PMSM. For example, uncertainty plane of a single input, which is "one-order linear", is as follows:

$$\dot{x}(t) = Ax(t) + Bu(t) + \Omega \quad (9)$$

Here, $x(t)$ and $x(t) \in R^+$, $u(t)$ are the output and the control actual, respectively. Also, $u(t) \in R^+$*A,B* could be the normal plane parameters. In addition, $A, B \in R^+$,**Ω** represents lumped uncertainty such as the unknown modeled external disturbance uncertainties and uncertainties. They are bounded to satisfy "$|\Omega| \leq \Omega_{max}, \Omega_{max} \in R^+$, R^+"represents several positive real limits. In this model, the regulation problem means obtaining a proper control input $u(t)$ with the outcome tracks of a positive command asymptotically. The tracking error$e(t)$, $e(t) \in R$, regarding the command output signal $x^*(t)$,$x^*(t) \in R$, with calculated real outcome signal are $x(t), x^*(t) \in R$

$$e(t) = x^*(t) - x(t) \quad (10)$$

3.1. Switching plane design

One of the crucial step of SMC design is constructing "sliding surface" *s*(*t*), $s(t) \in R$. A "2nd order sliding mode" when $(t) = \dot{s}(t) = 0$ is a sliding mode ". The second sliding mode aims at steering the state (error) for moving on the surface of the switching *s*(*t*) = 0. It also helps keeping its first successive derivative $\dot{s}(t) = 0$. In this case, the issue is the generation of a SO-SMC within selected surface *s*(*t*) where the chosen PI sliding plane that has coefficients that are constant are:

$$\mathbf{s}(\mathrm{t}) = \mathrm{e}(\mathrm{t}) + \mathrm{k_i} \int_0^{\mathrm{t}} \mathrm{e}(\tau)\mathrm{d}\tau \quad (11)$$

Here, k_i, $k_i \in R^+$ could stand for the integral independent positive parameter of output. The trapping of the system occurred near the surface where sliding occurs, in particular $s(t) = \dot{s}(t) = 0$, (11) as:

$$e(t) + k_i \int_0^t e(\tau)d\tau = 0 \quad (12)$$

The ordinary differential equations could provide the equation roots (12):

$$e(t) = \exp(-k_i) + \delta \quad (13)$$

Where δ ,$\delta \in R^+$ could be the positive constant. The above equation includes the tracking error *e*(*t*) convergence to zero drastically when there is proper choice of the constant coefficient k_i. Thus, equation (12) is limited to polynomial Hurwitz with roots strict in the complex plane open left side. Thus, $e(t) = 0$ and this indicates the close-loop system becomes universally asymptotically constant[26, 27].

3.2. Switch control design

To find the feedback control, followings are taken:

$$u = \Psi(s, \dot{s}) \quad (14)$$

The convergences of the trajectories could happen in the origin finite time to $s(t) = \dot{s}(t) = 0$ in the phase plane of $s, \dot{s}$. Thus, the occurrence of the primary error anywhere other than the sliding surface *s*(*t*), or the derivation of the representative of the *s*(*t*) caused by the variable differences and disturbances forces the switching control law to take the error to the *s*(*t*) till it is in $s(t)$ in the reaching phase. For avoiding the chattering phenomena, the use of a PI-based sliding function could smooth the switching course. The PI-based sliding surface control law could be as follows:

$$\mu(\mathrm{s}, \dot{\mathrm{s}}) = \gamma_1 \mathrm{sign}(\mathrm{s}) + \gamma_2 \mathrm{sign}(\dot{\mathrm{s}}) \quad (15)$$

Here, γ_i stands for a positive constant, $\gamma_i \in R^+$, and *sign*(.) is a sign function:

$$sign(s) = \{1, s > 0\ 0, s = 0\ -1\ s < 0\} \quad (16)$$

The control law convergence condition (13) is [19]:

$$(\gamma_1 + \gamma_2)k_m - c > (\gamma_2 - \gamma_1)k_m + c$$

$$(\gamma_2 - \gamma_1)k_m > c \quad (17)$$

Here, $A \le C$, $0 \le K_m \le B \le K_M$, $C \in R^+$, $K_m, K_M \in R^+$

4. Design of sliding mode observer

The rotor angle observer accuracy is a main factor affecting the sensorless drive performance. This effect is caused by the robustness to the parameters of the differences and disturbance declining capabilities and the stationary adaptive observers ($\alpha\ \beta$) [28-30]or rotating (dq) [31, 32] frame. Yet, a single reference frame shows these observers (speed adaptive) producing a rotor-speed-dependent parameter. When there is a digital recognition, the adaption of the speed could often be conducted in the estimation process step. Then, the cumulative errors, delays and noises affects the speed estimate. The inaccurate speed feedback to the observer could worsen the speed evaluation and flux slowly. This could shake the drive, in particular, at low speeds. In Fig.2, the new SMO block diagram use is shown. Also, a constant reference frame includes the observed motor from the SMO with an alpha and a beta whose observed-actual motor current differences undergo a sign function. An LPF application on the sign function output could help in obtaining the equivalent values of EMF e_α and e_β within the stationary reference frame. Finally, the place of the rotor is tested by the determining the arctangent negative of the equivalent alpha component: SMO is

$$\begin{bmatrix} \dot{\hat{i}}_\alpha \\ \dot{\hat{i}}_\beta \end{bmatrix} = \frac{1}{L_q}\begin{bmatrix} v_\alpha \\ v_\beta \end{bmatrix} - \frac{R}{L_q}\begin{bmatrix} \hat{i}_\alpha \\ \hat{i}_\beta \end{bmatrix} - \frac{K_{SM}}{L_q}\begin{bmatrix} sign(\hat{i}_\alpha - i_\alpha) \\ sign(\hat{i}_\beta - i_\beta) \end{bmatrix} \quad (18)$$

Where

K_{SM} constant observer.

$\hat{i}_\alpha$ is observer α-axis current

$\hat{i}_\beta$ stands for observer β-axis current

The variables of the position-dependent are:

$$v_\alpha = R.i_\alpha + \frac{d}{dt}L_q i_\alpha + \frac{d}{dt}\lambda_\alpha' \quad (19)$$

$$v_\beta = R.i_\beta + \frac{d}{dt}L_q i_\beta + \frac{d}{dt}\lambda_\beta' \quad (20)$$

Using the relationship

$$i_\alpha = i_d \cos\theta - i_q \sin\theta \quad (21)$$

$$i_\beta = i_d \sin\theta + i_q \cos\theta \quad (22)$$

The equivalent EMF terms can be described and derived as follows:

$$e_\alpha' = \frac{d\lambda_\alpha'}{dt} = -\left(2L_1 i_d \omega + \omega\lambda_{pm}\right)\sin\theta \quad (23)$$

$$e_\beta' = \frac{d\lambda_\beta'}{dt} = -\left(2L_1 i_d \omega + \omega\lambda_{pm}\right)\cos\theta \quad (24)$$

The arrangement of (19) and (20) and their combination with (21) and (22) could give:

$$\begin{bmatrix} \dot{i}_\alpha \\ \dot{i}_\beta \end{bmatrix} = \frac{1}{L_q}\begin{bmatrix} v_\alpha \\ v_\beta \end{bmatrix} - \frac{R}{L_q}\begin{bmatrix} i_\alpha \\ i_\beta \end{bmatrix} - \frac{1}{L_q}\begin{bmatrix} e_\alpha{}' \\ e_\beta \end{bmatrix} \qquad (25)$$

Then, the subtraction (18) from (25) produces the error dynamics in the $s(t)$:

$$\begin{bmatrix} \dot{\bar{i}}_\alpha \\ \dot{\bar{i}}_\beta \end{bmatrix} = -\frac{R}{L_q}\begin{bmatrix} \bar{i}_\alpha \\ \bar{i}_\beta \end{bmatrix} + \frac{1}{L_q}\begin{bmatrix} e_\alpha{}' \\ e_\beta \end{bmatrix} - \frac{K_{SM}}{L_q}\begin{bmatrix} sign(\bar{i}_\alpha) \\ sign(\bar{i}_\beta) \end{bmatrix} \qquad (26)$$

Then, the errors of the observation can be obtained:

$$\bar{i}_\alpha = \hat{i}_\alpha - i_\alpha \qquad (27)$$

$$\bar{i}_\beta = \hat{i}_\beta - i_\beta \qquad (28)$$

This is followed by Lyapunov function:

$$V = \frac{1}{2}(\bar{i}_\alpha^{-2} + \bar{i}_\beta^{-2}) \qquad (29)$$

Then

$$\dot{V} = \bar{i}_\alpha.\dot{\bar{i}}_\alpha + \bar{i}_\beta.\dot{\bar{i}}_\beta = -\frac{R}{L_q}(\bar{i}_\alpha^{-2} + \bar{i}_\beta^{-2}) + \frac{1}{L_q}(e'_\alpha.\bar{i}_\alpha + e'_\beta.\bar{i}_\beta) - \frac{K_{SM}}{L_q}\left(\left|\bar{i}_\alpha\right| + \left|\bar{i}_\beta\right|\right). \qquad (30)$$

In (34), when there is a large enough K_{SM}, the following is used:

$$K_{SM} > \max\left\{\left|e'_\alpha\right|, \left|e'_\beta\right|\right\} \qquad (31)$$

Thus, the $\dot{V} < 0$ is often taken for guaranteed till $\bar{i}_\alpha = 0$ and $\bar{i}_\beta = 0$. The equivalent EMF vector often aligns with that of the actual EMF. The two EMF vectors differ because of the machine saliency. Also, this saliency, which is bound, makes the actual EMF and the term and the equivalent EMF components bound. The trajectory of the system remains in sliding surface and moving to the source. The expected current convergence with the "actual current" in the $s(t)$ of the sliding manifold state trajectory makes an interval of the finite time. The amount of the observed current of the measured value is forced by the convergence of the sliding-mode, which put, by the constant reference frame, the desired error values in the middle of the observed current value and that of the actual. In addition, *ia* and *ib* is set to zero with an equivalent regulation approach [33-36], which Fig.2 shows, are applied. Setting the error values, *ia* and *ib*, to zero expresses the equivalent EMF as follows

$$\left[K_{SM}\, sign\left(\bar{i}_\alpha\right)\right]_{eq} = e'_\alpha \qquad (32)$$

$$\left[K_{SM}\, sign\left(\bar{i}_\beta\right)\right]_{eq} = e'_\beta \qquad (33)$$

The use of the low-pass filters (LPFs) for the extraction of e_α and e_β helps position estimations. Finally, to get the rotor position, the following is used:

$$\hat{\theta} = -\tan^{-1}\left(\frac{e'_{\alpha}}{e'_{\beta}}\right) = -\tan^{-1}\left(\frac{\left[K_{SM}\, sign\left(\bar{i}_{\alpha}\right)\right]_{eq}}{\left[K_{SM}\, sign\left(\bar{i}_{\beta}\right)\right]_{eq}}\right) \qquad (34)$$

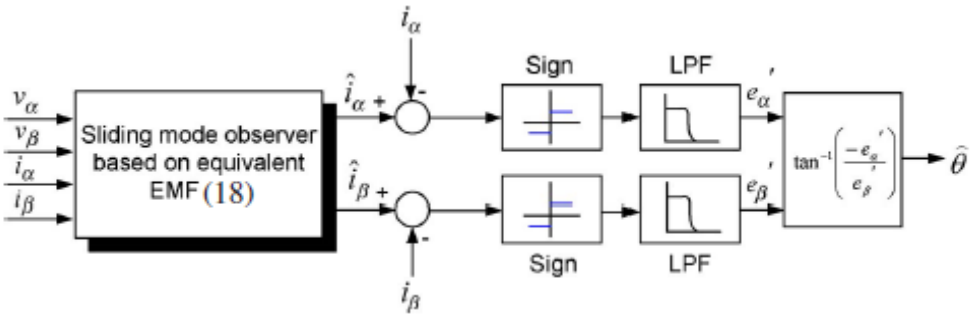

Figure 2. A SMO based equivalent EMF Utilization

5. Simulation results

Fig.1 explains of the suggested control and observer schemes in the control diagram use. The inputs are the current of the stationary reference frame. The inputs also include signals of voltage to the estimator of position. This is followed by the voltage reference of the current regulator outputs in the frame of the synchronous reference which returns to that of stationary reference. The reference frame transformation used by the current regulators creates *d*- and *q*-axis signals of the current feedback (*id* and *iq*).
If (5) is substituted into (7), one can obtain:

$$\dot{\omega} = A_r \omega_r + B_r i_q + k \qquad (35)$$

Were

$$A_r = J^{-1}B_m \;,\; B_r = \frac{3n_p L_{md} I_{df}}{2J}$$

Here, the lumped uncertainty includes unknown modeled uncertainties with external disturbance uncertainties, bounded to satisfy $k \le k_{max}$, $k_{max} \in R^+$, R^+ refers to positive real constants. Thus, (14) forces:

$$i_q = u\,(s, \dot{s}) \qquad (36)$$

The selection of the SO-SMC coefficients, γ_i , k_i helps testing the close-loop condition PMSM servo drive. Also, as design guidelines, it is recommended to use the real positive sliding mode controller parameters. This is the reaching condition. Here, the SO-SMC parameters in (11) and (15) become $k_i = 0.05$, $\gamma_1 = 22$, $\gamma_2 = 22.935$, for the SO-SMC for getting a higher accuracy.

Figure 3 is the simulation results. The results were obtained by the estimated position in which there was an equal EMF to close the current loops. These loops are known as the torque mode with no load) with $i_q^* = 8$ A and $i_d^* = 0$ A. The zoomed-in parts show the location of 2.9 to 2.95 s in red trace.

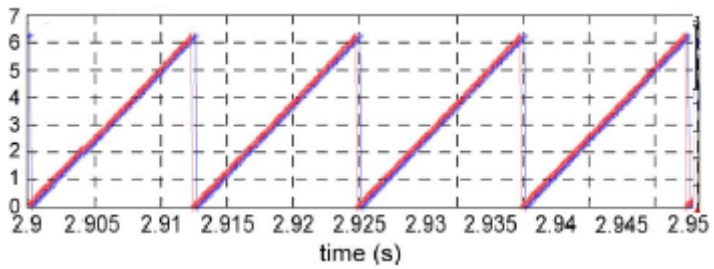

Figure 3. The use of the equivalent EMF with $i_d = 0$A and $i_q = 8A$ to obtain the results of the experiment in torque mode

Figs 4–6 show several speed-tracking experiments. They illustrate the performance of the new model in the motor using the speed trajectories selected with different shapes. Fig 4 shows the reference trajectory performance which the trapezoidal (Fig 4 a) and sinusoidal velocity profile (Fig 4 a) provide. In the speed transient, the speed transient is made by the shifts in the references. As Figure 4(a) explains, there is a good tracking performance in terms of the first order SMC. The errors of tracking appear in Figs. 4(b) .

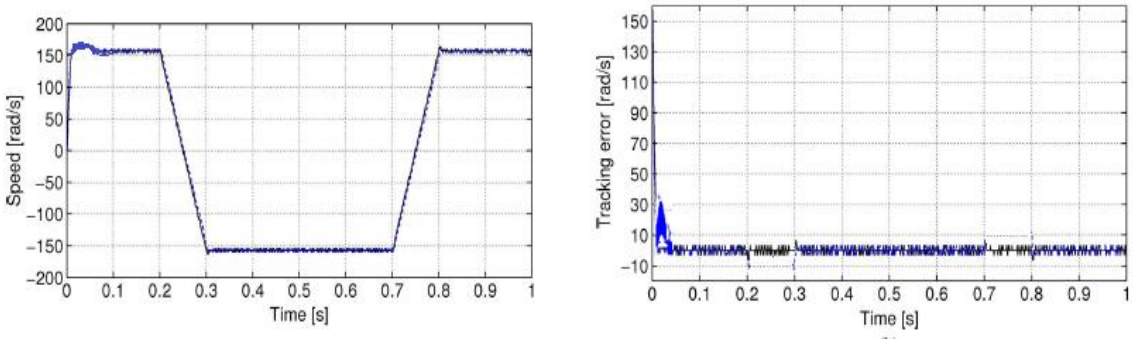

Figure 4. (a) Trapezoidal velocity profile, (b) Tracking error

For the evaluation of the SO-SMC robust performance, its tracking performances occurred when there are no external disturbances but sinusoid external disturbances. They are both tested. The suggested SO-SMC speed of the responses and the related regulation attempts of a sinusoidal reference trajectory command shifts. This shift has no external disturbances (Figure 4). Yet, there is a sinusoidal command change external disturbance (Figure 5). Tin the outcome of the control error and that of the tracking trajectory, the SMC remains accurate and robust SMC positive in its features.

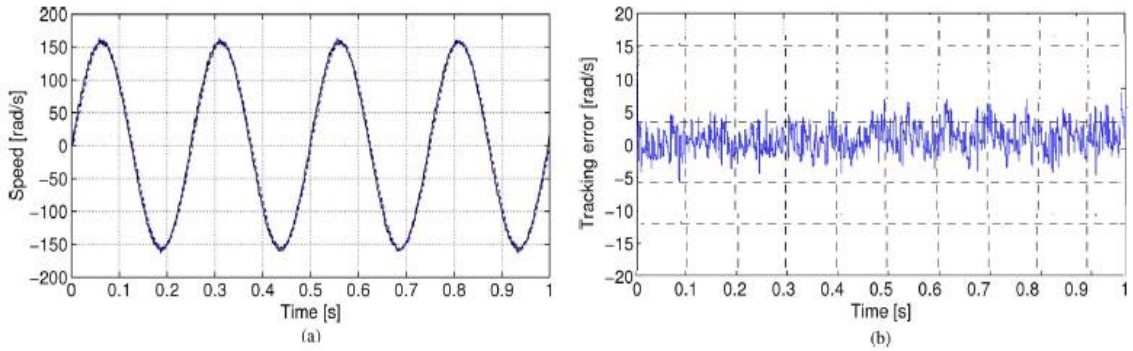

Figure 5. Profile of the Sinusoidal velocity. (a), The black continuous line superimposing PI-based FOC and reference velocity nearly finished). (b) Tracking error

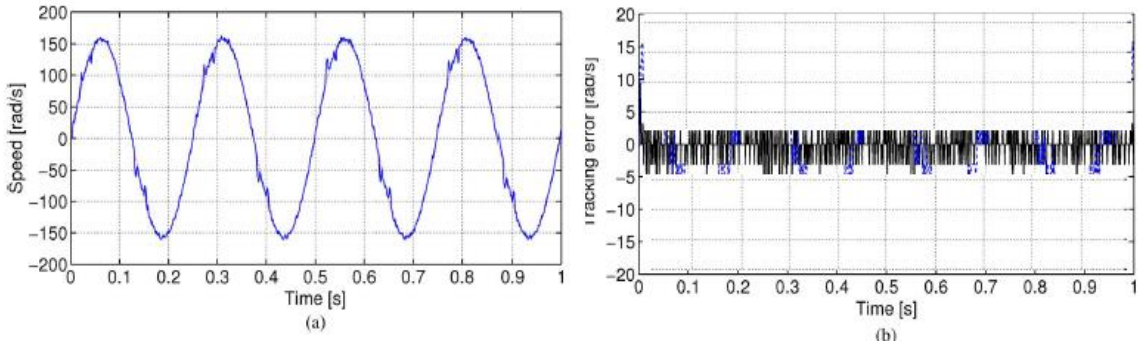

Figure 6. The SO-SMC with the sinusoidal disturbance simulation responses:
(a) Reference and actual speeds. (b) Error of the Trajectory

Table 1. Motor parameters

Motor Parameter	Value
Phase resistance	4.5 ohm
Phase inductance	3.5 mH
Back Emf constant	3 mv/rpm

Motor Parameter	Value
Rated speed	2000 rpm
Pole pair	2
λ_{pm}	0.66 Wb

6. Conclusions

The study proposed SO-SMC scheme according to the PI sliding plane. The standards were presented in the used FOC PMSM servo drive plane. Then the new SOSMC system discussed and examined in details. For the demonstrations of the effectiveness of the new scheme, the study conducted simulations. In addition, this work designed a novel SMO according to the equivalent EMF model. The novel model is different from other very difficult sliding observers for salient synchronous machines in being easy to use.

References

[1] Y. Wang, Q.-y. Wang, H. Pei, "Design of numerical control and realization of drive in soft CNC system," Computer Engineering and Design, vol. 30, pp. 1882-1885, 2009.

[2] J. U. Cho, Q. N. Le, and J. Jeon, "An FPGA-based multiple-axis motion control chip," *IEEE Transactions on Industrial Electronics,* vol. 56, no. 3, pp. 856-870, 2008.

[3] K. Jezernik, "High precision VSS motion control of servo drives," in *2008 10th IEEE International Workshop on Advanced Motion Control*, 2008, pp. 710-715: IEEE.

[4] S. Fang, B. Zhou, D. Li, "Servo control system for three-axis brushless flight simulator," *Journal of Nanjing University of Aeronautics & Astronautics*, pp. 701-705, 2007.

[5] K.-Y. Cheng and Y. Tzou, "Fuzzy optimization techniques applied to the design of a digital PMSM servo drive," *IEEE Transactions on Power Electronics,* vol. 19, no. 4, pp. 1085-1099, 2004.

[6] A. Ghazi, S. Aljunid, A. Fareed, S. Z. S. Idrus, C. M. Rashidi, A. Al-dawoodi, and A. M. Fakhrudeen, "Performance Analysis of ZCC-Optical-CDMA over SMF for Fiber-To-The-Home Access Network," in *Journal of Physics: Conference Series*, 2020, vol. 1529, no. 2, p. 022013: IOP Publishing.

[7] P. Xu and Z. Zhu, "Novel carrier signal injection method using zero-sequence voltage for sensorless control of PMSM drives," *IEEE Transactions on Industrial Electronics,* vol. 63, no. 4, pp. 2053-2061, 2015.

[8] Y. Shi, K. Sun, L. Huang, and Y. Li, "Online identification of permanent magnet flux based on extended Kalman filter for IPMSM drive with position sensorless control," *IEEE Transactions on Industrial Electronics*, vol. 59, no. 11, pp. 4169-4178, 2011.

[9] S. Chi, Z. Zhang, and L. Xu, "Sliding-mode sensorless control of direct-drive PM synchronous motors for washing machine applications," *IEEE Transactions on Industry Applications,* vol. 45, no. 2, pp. 582-590, 2009.

[10] A. Ghazi, S. Aljunid, S. Z. S. Idrus, C. Rashidi, A. Al-dawoodi, B. A. Mahmood, A. Fareed, M. U. Zaenal, N. H. Qasim, and R. M. Rafeeq, "A Systematic review of Multi-Mode Fiber based on Dimensional Code in Optical-CDMA," in *Journal of Physics: Conference Series*, 2021, vol. 1860, no. 1, p. 012016: IOP Publishing.

[11] H.. Naman, M. Al-dabag, H. Alrikabi, "Encryption System for Hiding Information Based on Internet of Things," *International Journal of Interactive Mobile Technologies (iJIM)*, vol. 15, no. 2, 2021.

[12] H. Kim, J. Son, and J. J. I. T. o. I. E. Lee, "A high-speed sliding-mode observer for the sensorless speed control of a PMSM," vol. 58, no. 9, pp. 4069-4077, 2010.

[13] M. A. a. Roa'a, I. A. Aljazaery, S. K. Al_Dulaimi, H. T. S. Alrikabi, and Informatics, "Generation of High Dynamic Range for Enhancing the Panorama Environment," *Bulletin of Electrical Engineering*, vol. 10, no. 1, 2021.

[14] Y. Jiang, W. Xu, C. Mu, and Y. Liu, "Improved deadbeat predictive current control combined sliding mode strategy for PMSM drive system," *IEEE Transactions on Vehicular Technology,* vol. 67, no. 1, pp. 251-263, 2017.

[15] G. Wang, T. Li, G. Zhang, X. Gui, and D. Xu, "Position estimation error reduction using recursive-least-square adaptive filter for model-based sensorless interior permanent-magnet synchronous motor drives," *IEEE transactions on industrial electronics,* vol. 61, no. 9, pp. 5115-5125, 2013.

[16] N. A. Hussien, H. Salim, F. Abed, "Monitoring the Consumption of Electrical Energy Based on the Internet of Things Applications," *International Journal of Interactive Mobile Technologies (iJIM),* vol. 15, no. 7, 2021.

[17] Chee-Mun Ong ,"Dynamic simulation of electric machine," *Printic Hall PTR,Upper Saddle River,New Jersey,*1998.

[18] D. Liang, J. Li, and R. Qu, "Super-twisting algorithm based sliding-mode observer with online parameter estimation for sensorless control of permanent magnet synchronous machine," in *2016 IEEE Energy Conversion Congress and Exposition (ECCE)*, 2016, pp. 1-8: IEEE.

[19] A. G. M. Al-dawoodi, M. Mahmuddin, "An empirical study of double-bridge search move on subset feature selection search of bees algorithm," *Journal of Telecommunication, Electronic and Computer Engineering,* vol. 9, no. 2-2, pp. 11-15, 2017.

[20] F. T. Abed, H. T. Salim Alrikabi, and I. A. Ibrahim, "Efficient energy of smart grid education models for modern electric power system engineering in Iraq," in *IOP Conference Series: Materials Science and Engineering*, 2020, vol. 870.

[21] P. Mercorelli, "A two-stage sliding-mode high-gain observer to reduce uncertainties and disturbances effects for sensorless control in automotive applications," *IEEE Transactions on Industrial Electronics,* vol. 62, no. 9, pp. 5929-5940, 2015.

[22] T. Bernardes, V. F. Montagner, H. A. Gründling, and H. Pinheiro, "Discrete-time sliding mode observer for sensorless vector control of permanent magnet synchronous machine," *IEEE Transactions on Industrial Electronics,* vol. 61, no. 4, pp. 1679-1691, 2013.

[23] A. Al-Dawoodi, H. MARAHA, S. ALSHWANI, A. GHAZI, A. M. FAKHRUDEEN, S. ALJUNID, S. Z. S. IDRUS, A. A. MAJEED, K. A. J. J. o. E. S. AMEEN, and Technology, "Investigation of 8 x 5 Gb/s mode division multiplexing-fso system under different weather condition," *Journal of Engineering Science and Technology,* vol. 14, no. 2, pp. 674-681, 2019.

[24] N. A. jassim. H. Th., "Design and Implementation of Smart City Applications Based on the Internet of Things," *iJIM*, vol. 15, no. 3, 2021.

[25] M. Al-dabag, H. S. ALRikabi, and R. Al-Nima, "Anticipating Atrial Fibrillation Signal Using Efficient Algorithm," *International Journal of Online and Biomedical Engineering (iJOE),* vol. 17, no. 2, pp. 106-120, 2021.

[26] I. Eker, "Second-order sliding mode control with experimental application," *ISA transactions,* vol. 49, no. 3, pp. 394-405, 2010.

[27] B. K. Mohammed, M. B. Mortatha, A. S. Abdalrada, and H. ALRikabi, "A comprehensive system for detection of flammable and toxic gases using IoT," *Periodicals of Engineering and Natural Sciences*, vol. 9, no. 2, pp. 702-711, 2021.

[28] K. Liu and Z. Zhu, "Position-offset-based parameter estimation using the adaline NN for condition monitoring of permanent-magnet synchronous machines," *IEEE Transactions on Industrial Electronics,* vol. 62, no. 4, pp. 2372-2383, 2014.

[29] J. Davila, L. Fridman, and A.. Levant, "Second-order sliding-mode observer for mechanical systems," *IEEE transactions on automatic control*, vol. 50, no. 11, pp. 1785-1789, 2005.

[30] S. Morimoto, K. Kawamoto, M. Sanada, and Y. Takeda, "Sensorless control strategy for salient-pole PMSM based on extended EMF in rotating reference frame," *IEEE transactions on industry applications,* vol. 38, no. 4, pp. 1054-1061, 2002.

[31] Z. Chen, M. Tomita, S. Doki, and S. Okuma, "An extended electromotive force model for sensorless control of interior permanent-magnet synchronous motors," *IEEE transactions on Industrial Electronics*, vol. 50, no. 2, pp. 288-295, 2003.

[32] S. Morimoto, M. Sanada, and Y. Takeda, "Mechanical sensorless drives of IPMSM with online parameter identification," vol. 42, no. 5, pp. 1241-1248, 2006.

[33] Z. Yan and V. Utkin, "Sliding mode observers for electric machines-an overview," in *IEEE 2002 28th Annual Conference of the Industrial Electronics Society. IECON 02*, 2002, vol. 3, pp. 1842-1847: IEEE.

[34] H. Tuama, H. Abbas, N. S. Alseelawi, and H. T. S. ALRikabi, "Bordering a set of energy criteria for the contributing in the transition level to sustainable energy in electrical Iraqi Projects," *Periodicals of Engineering and Natural Sciences,* vol. 8, no. 1, pp. 516-525, 2020.

[35] Y. Zhang, P. Stansby, and G. Li, "Non-causal linear optimal control with adaptive sliding mode observer for multi-body wave energy converters," *IEEE Transactions on Sustainable Energy,* vol. 12, no. 1, pp. 568-577, 2020.

[36] S. Asadi, A. Khayatian, M. Dehghani, N. Vafamand, and M. Khooban, "Robust sliding mode observer design for simultaneous fault reconstruction in perturbed Takagi-Sugeno fuzzy systems using non-quadratic stability analysis," *Journal of Vibration and Control,* vol. 26, no. 11-12, pp. 1092-1105, 2020.